Mon. Not. R. Astron. Soc. **000**, 000–000 (0000) Printed 11 September 2000 (MN LATEX style file v1.4)

Linear and nonlinear contributions to pairwise peculiar velocities

Ravi K. Sheth[1], Lam Hui[2,3], Antonaldo Diaferio[4] & Román Scoccimarro[2]

[1] *NASA/Fermilab Astrophysics Group, MS 209, Batavia, IL 60510-0500*
[2] *Institute for Advanced Study, School of Natural Sciences, Einstein Drive, Princeton, NJ 08540*
[3] *Department of Physics, Columbia University, 538 West 120th Street, New York, NY 10027*
[4] *Dipartimento di Fisica Generale "Amedeo Avogadro", Universitá di Torino, Italy*
Email: sheth@fnal.gov, lhui@ias.edu, scoccima@ias.edu, diaferio@ph.unito.it

Submitted to MNRAS 2000 August 15

ABSTRACT

We write the correlation function of dark matter particles, $\xi(r)$, as the sum of two terms—one which accounts for nonlinear evolution, and dominates on small scales, and another which is essentially the term from linear theory, and dominates on large scales. We use models of the number and spatial distribution of haloes and halo density profiles to describe the nonlinear term and its evolution. The result provides a good description of the evolution of $\xi(r)$ in simulations. We then use this decomposition to provide simple and accurate models of how the single particle velocity dispersion evolves with time, and how the first and second moments of the pairwise velocity distribution depend on scale. The key idea is to use the simple physics of linear theory on large scales, the simple physics of the virial theorem on small scales, and our model for the correlation function to tell us how to weight the two types of contributions (linear and nonlinear) to the pairwise velocity statistics. When incorporated into the streaming model, our results will allow a simple accurate description of redshift-space distortions over the entire range of linear to highly nonlinear regimes.

Key words: galaxies: clustering – cosmology: theory – dark matter.

1 INTRODUCTION

Strong constraints on models of large scale structure follow from combining statistics of the density field with statistics of the velocity field. In this paper, we show how the number of particle pairs depends on pair separation, and use this to compute the mean and mean square pairwise velocity. That is, we show how the correlation function of the density field and the distribution of pairwise velocities can all be computed from the same model.

The key to being able to do this is a simple model of how and why the correlation function $\xi(r, a)$ evolves with time. The evolution of ξ was first accurately modelled by Hamilton et al. (1991). Following Peebles (1980), they showed that knowledge of how the correlation function evolved allowed them to describe how the mean streaming velocity $v_{12}(r, a)$ of particle pairs evolved as well (also see Nityananda & Padmanabhan 1994). Peebles suggests that the second moment of the pairwise distribution, $\sigma_{12}(r, a)$ depends on (an integral over) the three-point correlation function $\zeta(r, a)$; because there is no general description of ζ from linear to non-linear scales (but see Scoccimarro & Frieman 1998 for scale-free initial conditions), there is, at present, no simple description of how the pairwise velocity dispersion depends on scale (see, e.g., Mo, Jing & Börner 1997; Jing, Mo & Börner 1998).

In this paper, we will follow a different approach than the one laid down by Hamilton et al. The logic behind our approach follows from the models first discussed by Neyman & Scott (1959), and references therein. In these models, all particles are assumed to be in collapsed haloes, and the correlation function of the particles depends on the density profiles as well as on the spatial distribution of the parent haloes. What has changed since those early days is that we now understand that, for statistics like the correlation function, the most important parameter of a halo is its mass.

Following Sheth & Saslaw (1994), Sheth & Jain (1997) showed that they were able to provide a good description of the dark matter correlation function on small scales even though they neglected the fact that the parent haloes are clustered. This works because most close pairs are actually in the same halo, and so the correlation function depends only on the distribution of particles within haloes (the halo density profile) and not on the spatial distribution of the other haloes. Using formalism presented in McClelland & Silk (1977), they showed how to write the correlation function as an integral over haloes having a range of

masses. They then used simple analytic approximations for $n(m)$, the number density of haloes (the mass function formula of Press & Schechter 1974), and halo density profiles (power-laws with slopes chosen to agree with simulations), to present their results.

The results of e.g., Scherrer & Bertschinger (1991), show that one really expects the power-spectrum to be the sum $P_{\rm 1halo}(k) + P_{\rm 2halo}(k)$, where $P_{\rm 2halo}(k)$ is the contribution from pairs in different haloes (i.e., the term that was neglected by Sheth & Jain). More recently, Seljak (2000) and Peacock & Smith (2000) have extended the model calculation to include these terms. They used slightly more accurate fitting formulae for the inputs (the mass function is from Sheth & Tormen 1999 and the halo profiles are from the work of Navarro, Frenk and White 1997). Their results show that a good approximation to the evolved $P(k)$ on all scales can be got by simply setting $P_{\rm nl}(k) = P_{\rm 1halo}(k) + P_0(k)$, where the first term is that due to the halo profiles and mass function, and the second is the initial power-spectrum evolved to the present time using linear theory.

Section 2 of this paper studies the two-point correlation function, $\xi(r)$, rather than its Fourier transform, $P(k)$. Of course, in this case also, $\xi(r) = \xi_{\rm 1halo}(r) + \xi_{\rm 2halo}(r)$, but we feel that explicitly working in real space shows the sorts of approximations which lead to this decomposition more clearly. It also shows why, both in real and in Fourier space, the 2-halo term should approximately equal the linear theory expression.

Since this is a model in which the contributions to $\xi(r)$ are written as functions of halo mass, we can study the Layzer-Irvine cosmic energy equation as a function of halo mass. We show this in Section 3. Our analysis shows which terms in the energy equation come from nonlinear virial motions within each halo, and which from the motions of haloes as a whole which, following Sheth & Diaferio (2000), are more in line with what the linear theory would predict. We show how our decomposition allows us to provide a simple estimate of the single particle velocity dispersion—which can be thought of as the density weighted temperature.

The requirement of pair conservation provides a relation between the correlation function $\xi(r)$ and the first moment of the pairwise velocity distribution $v_{12}(r)$. In Section 4 we use our decomposition of ξ to provide a simple expression for the mean streaming velocity, v_{12}, and then show that this expression describes measurements in simulations quite well.

Peebles (1980) shows that the second moment, $\sigma_{12}(r)$, is related to (an integral over) the three-point correlation function, ζ. This relation between the pairwise dispersion and ζ is often called the cosmic virial theorem. Since our halo-based approach allows us to model ζ as well (Scoccimarro et al. 2000), we could, in principle, use this to study how $\sigma_{12}(r)$ depends on pair separation. In Section 5 we describe what we think is a much simpler way to think about and model $\sigma_{12}(r)$. In our approach, the important ingredient is not ζ, but knowledge of how velocities are correlated. We first show that neglecting these correlations is a rather good approximation: our models of ξ and the single particle velocity dispersion are sufficient for describing the main features of σ_{12}. We then describe a simple model for including the effects of velocity correlations.

Knowledge of both the mean and the dispersion of pairwise velocities are useful for modelling redshift space distortions, which we plan to present elsewhere. The three velocities we study here, the single particle velocity dispersion $\langle v^2\rangle$, the mean streaming velocity $v_{12}(r)$, and the pairwise dispersion $\sigma^2_{12}(r)$ may all be used to provide estimates of the density of the Universe, although Jenkins et al. (1998) discuss why, in cluster normalized CDM models, different cosmological models may have rather similar values of v_{12} and σ_{12}.

2 THE CORRELATION FUNCTION

Let $\rho(r|m)$ denote the shape of the density profile of a halo which contains mass m; the mass in a spherical shell at distance r from the centre of the halo is $4\pi r^2\,\rho(r|m)\,{\rm d}r$. Let $\lambda(r|m)$ denote the convolution of such a profile with another of exactly the same shape. For spherically symmetric density profiles

$$\lambda(r|m) \equiv 2\pi \int {\rm d}x_1\; x_1^2\,\rho(x_1|m) \int_{-1}^{1} {\rm d}\beta\;\rho(x_2|m), \qquad (1)$$

where $x_2^2 = x_1^2 + r^2 - 2x_1 r\beta$. The contribution to the correlation function from pairs in which both particles are in the same halo is given by weighting the convolution profile of a halo of mass m by the number of haloes of mass m, and integrating over m (Sheth & Jain 1997). The total correlation function is the sum of this plus a term which arises from pairs which are in two different haloes. This means that the second term is a convolution of the profiles of each of the two haloes involved, with the halo-halo correlation function:

$$\Lambda(r|m_1,m_2) \;=\; \int {\rm d}^3r_1 \int {\rm d}^3r_2\;\rho(r_1|m_1)\rho(r_2|m_2) \times\; \xi_{\rm hh}\Big(|r_1 - r_2 + r|\,\Big|m_1,m_2\Big). \qquad (2)$$

Suppose that the halo-halo correlation function changes slowly on separations which are large compared to the typical size of a halo. Then, at large r, the halo-halo correlation function can be taken outside the integrals, leaving just the convolutions over the profiles. But these each contribute a factor which equals the mass of the halo, since any position within the halo gives approximately the same pair separation. This means that

$$\Lambda(r|m_1,m_2) \approx m_1\,m_2\;\xi_{\rm hh}(r|m_1,m_2) \qquad (3)$$

at large separations.

To proceed, we need a model for $\xi_{\rm hh}(r|m_1,m_2)$. This has been done by Mo & White (1996) and Sheth & Lemson (1999). On large scales, Mo & White argued that the correlation function of haloes of mass m should simply be a constant times the correlation function of the dark matter, $\xi_{\rm hh}(r) = b^2(m)\,\xi(r)$, and that the value of the constant should depend on the halo mass. Sheth & Tormen (1999) showed that this dependence on mass can be derived from the shape of the mass function $n(m)$, which, in turn, depends on the initial shape of the power spectrum. In addition, on large scales, linear theory should apply, and so $\xi(r) \approx \xi_0(r)$, where $\xi_0(r)$ is the linear theory correlation function of the dark matter. Thus, for large separations,

$$\xi_{\rm hh}(r|m_1,m_2) \approx b(m_1)\,b(m_2)\;\xi_0(r). \qquad (4)$$

On small scales the halo-halo correlation function must eventually turn over (haloes are spatially exclusive—so each halo is like a small hard sphere). So setting $\xi_{\rm hh}(r|m_1,m_2) \approx b(m_1)\,b(m_2)\,\xi(r)$ will almost surely overestimate the true value. Using the linear, rather than the nonlinear correlation function, even on small scales, is a crude but convenient way of accounting for this overestimate. (Although the results of Sheth & Lemson 1999 allow one to account for this more precisely, it turns out that great accuracy is not really needed since, on small scales, the correlation function is determined almost entirely by the one-halo term anyway.)

If we allow a range in halo masses then the total correlation function is

$$\begin{aligned}\xi(r) &\equiv \xi_{\rm 1halo}(r) + \xi_{\rm 2halo}(r) \\ &= \int {\rm d}m\,\frac{n(m)}{\bar\rho}\,\frac{\lambda(r|m)}{\bar\rho} + \\ &\quad \int {\rm d}m_1\,\frac{n(m_1)}{\bar\rho}\int {\rm d}m_2\,\frac{n(m_2)}{\bar\rho}\,\Lambda(r|m_1,m_2), \qquad (5)\end{aligned}$$

where $n(m)\,{\rm d}m$ denotes the number density of haloes which have mass in the range ${\rm d}m$ about m, and $\bar\rho$ is the average density. The first term dominates on small scales, and the second term dominates on large separations. Now, on large scales $\Lambda(r|m_1,m_2)$ is well approximated by the product of $m_1\,b(m_1)$, $m_2\,b(m_2)$ and $\xi_0(r)$. We will not do too badly if we continue to use this approximation on smaller scales because the scales on which it breaks down are precisely those on which the first term begins to dominate. This means that the second term can be written as the product of two one dimensional integrals. Moreover, the bias factors are defined so that

$$\int {\rm d}m_1\,\frac{m_1 n(m_1)}{\bar\rho}\,b(m_1) \equiv 1. \qquad (6)$$

Therefore, the second term really is very simple: to a good approximation,

$$\xi(r) \approx \int {\rm d}m\,\frac{n(m)}{\bar\rho}\,\frac{\lambda(r|m)}{\bar\rho} + \xi_0(r). \qquad (7)$$

Note that, in this approximation, the second term is the same for all halo profiles—different profile shapes yield different shapes for $\lambda(r|m)$ and so result in different correlation functions on small scales only; in principle, one can use measurements of the shape of the correlation function at small separations to constrain the shapes of profiles.

To illustrate how the profile affects the correlation function, in what follows we will use the NFW profile of Navarro, Frenk & White (1997). In Appendix A we provide expressions for $\lambda(r|m)$ for the NFW profile truncated at the virial radius, the Hernquist profile (1990), and the singular isothermal sphere, truncated at the virial radius so that it has finite mass. These three density profiles all have the property that $\lambda(r|m)$ is never less than zero. As a result, $\xi_{\rm 1halo}$ is also never less than zero. This means that the integral of $\xi_{\rm 1halo}$ over all separations does not equal zero. As a result, equation (7) above does not satisfy the integral constraint. This is a formal feature of the models to which we will return later.

The truncated NFW profile above has two free parameters, a core radius and an average density. Navarro, Frenk & White (1997) showed that, in their simulations, the core radius depends on the mass of the halo, whereas all haloes have the same average density, whatever their mass. They found that the core radii of massive haloes are at larger fractions of their virial radii than for less massive haloes; less massive haloes are more centrally concentrated. The ratio of the core radius to the virial radius increases with mass in a way which depends on the shape of the initial power-spectrum—they discuss in detail why this is so. In what follows, we will use the simple analytic approximation to this relation given in Scoccimarro et al. (2000) as we integrate $\lambda(r|m)$ over the mass function: $a_{\rm NFW}(m) = (m/m_*)^{0.13}/9$, where m_* is the average mass contained in a tophat filter whose scale is set by the requirement that the rms value of the initial density fluctuation field smoothed with the filter, extrapolated to the present using linear theory, is $\delta_{\rm c} \approx 1.68$.

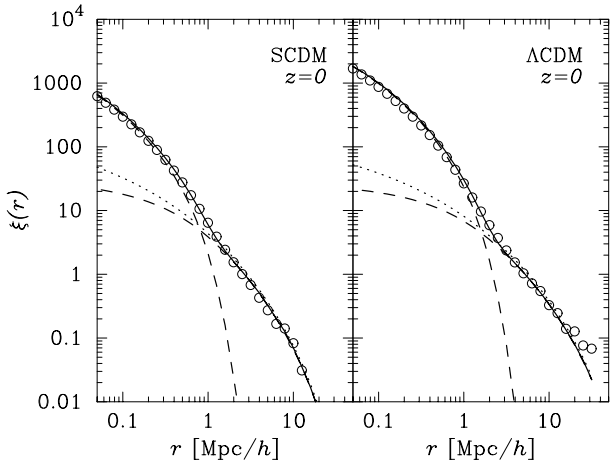

Figure 1. The correlation function of dark matter particles. Symbols show the fitting formula provided by Peacock & Dodds (1996). Solid curves show the correlation associated with NFW profiles. The two dashed curves show the contribution from pairs in the same halo (dominates at small r), and pairs in different haloes (dominates at large r). Dotted curve shows the linear theory correlation function ξ_0; on the large scales where the two-halo term dominates, it is very well approximated by the linear theory function.

Fig. 1 shows the correlation functions one obtains by inserting the core-radius relation given above into our expressions for $\lambda(r|m)$, and integrating over the mass function. The two panels show two variants of the CDM family of initial conditions: our SCDM model has $\Omega_0 = 1$, $h = 0.5$ and $\sigma_8 = 0.5$, whereas our ΛCDM model has $\Omega_0 = 1$, $\Lambda_0 = 1 - \Omega_0$, $h = 0.7$ and $\sigma_8 = 0.9$. The symbols show the fitting formula of Peacock & Dodds (1996) which describes the correlation functions from numerical simulations of these cosmological models well (see, e.g., Mo, Jing & Börner 1997; Jenkins et al. 1998), and the solid curve shows our model using NFW profiles. The two dashed curves, which sum to give the solid curve, show the two contributions to the correlation function; the curve which dominates on small scales shows the contribution from pairs in the same halo—the first term in equation (5). The curve which dominates on large scales shows the contribution from pairs in different haloes. The dotted curve shows the linear theory correlation function; on the scales where the two-halo term dominates, the linear theory function provides an excellent approximation. The model provides a good description of the correlation func-

tion of the dark matter. Although we have only presented results for $z = 0$, the model is also accurate at earlier times.

3 THE COSMIC ENERGY EQUATION

The cosmic energy equation describes how the energy of the Universe is partitioned between kinetic and potential energy. In essence, it provides a relation between the correlation function of dark matter particles and their rms speeds. Following Hamilton et al. (1991), we know how to compute the shape of the correlation function (i.e., how it depends on separation r) at any time, if its initial shape is known (also see Nityananda & Padmanabhan 1994). Mo, Jing & Börner (1997) showed that inserting this evolution into the cosmic energy equation provided a very good description of how the rms velocities of dark matter particles in their simulations evolved. How much of the evolution of the rms velocity is driven by nonlinear effects within virialized clusters, which produce large velocities, and how much contains information about the (linearly evolved) initial conditions? We show below that the model described above allows us to separate out the linear from the nonlinear effects.

The cosmic energy equation (Irvine 1961, 1965; Layzer 1963, 1964) is an exact statement of what energy conservation means in an expanding universe. It provides a relation between the potential energy of the system,

$$W(a) = -2\pi G\bar{\rho}(a) \int \mathrm{d}r\ r\,\xi(r,a), \tag{8}$$

and the kinetic energy $K(a)$, which is essentially one half times the mean square velocity of the particles in the system. (Note that $\bar{\rho} \propto a^{-3}$, where a denotes the scale factor of the Universe, and not the core radius of the halo profile!) If the evolution of W is known, then the cosmic energy equation allows one to compute the evolution of K also. Since we know how $\xi(r,a)$ evolves, we know how W evolves, so we can compute $K(a)$ also. Mo, Jing & Börner (1997) showed that by combining the Hamilton et al. (1991) evolution of $\xi(r,a)$ with the cosmic energy equation they were able to compute a good approximation to the value of the single particle velocity dispersion at any given time. In particular, by integrating the energy equation once, Mo et al. (1997) showed that

$$\langle v^2(a)\rangle = \frac{3}{2}\,\Omega(a)H^2(a)\,a^2 I(a)\left(1 - \int_0^a \frac{I(a')}{I(a)}\,\frac{\mathrm{d}a'}{a}\right), \tag{9}$$

where $W(a) = -2\pi G\bar{\rho}(a)\,a^2 I(a)$. Although this expression is exact, Mo et al. also showed that the simpler expression which follows if $I(a) \propto D(a)^2$, as it would in linear theory, is a good approximation: In this case

$$\langle v^2(a)\rangle \approx \frac{3}{2}\,\Omega(a)H^2(a)\,a^2 I(a)\left(1 - \int_0^a \frac{D^2(a')\,\mathrm{d}a'}{aD^2(a)}\right). \tag{10}$$

Davis, Miller & White (1997) were interested in separating out those contributions to the velocity dispersion which arise from nonlinear effects from those which are given by linear theory. Since we know how to write $\xi(r,a)$ as a sum of two terms, one from linear theory and the other nonlinear, we can begin to address some of the issues they raised. Specifically, suppose we write

$$W = W_{\rm linear} + W_{\rm nonlinear} \tag{11}$$

and we require that it equals the expression for W above. Linear theory, extrapolated to the present time, would have

$$W(a) = -2\pi G\bar{\rho}(a) \int \mathrm{d}r\ r\,\xi_0(r), \tag{12}$$

where ξ_0 denotes the linear correlation function (e.g. Peebles 1980). However, our model for the nonlinear correlation function is to write $\xi(r)$ as a sum of this linear part, plus a term which depends on halo profiles. Thus, we find that

$$W_{\rm nonlinear} = -2\pi G \int \mathrm{d}m\ \frac{n(m)}{\bar{\rho}} \int \mathrm{d}r\ r\,\lambda(r|m). \tag{13}$$

where we have rearranged the order of the integrals so that we do do the one over r before integrating over m. The resulting integrals over r are computed explicitly in the Appendix. In particular, for the halo models of interest in this paper, the haloes are in virial equilibrium: $W_{\rm nonlinear} = -2K_{\rm nonlinear}$. Thus, in our approach, the ratio of the nonlinear to the linear theory term depends on the mass function and the density profiles of dark matter haloes. For example, for NFW haloes, $-W_{\rm nonlinear}$ equals $\int \mathrm{d}m\,[n(m)/\bar{\rho}]\,(Gm^2/r_{\rm vir})$ times a constant which depends on the ratio of the core radius to the virial radius.

We will not explore this further in this paper. For the time being, we will simply use this expression to estimate how the single particle velocity dispersion evolves. Namely, we will use linear theory extrapolated to the present time to estimate $W_{\rm linear}$ (see, e.g., Peebles 1980) and our models of halo profiles to estimate the other contribution to $W_{\rm nonlinear}$, and we will then use the energy equation to derive $\langle v^2\rangle$. We will need this single particle $\langle v^2\rangle$ later on, when we study how the pairwise velocity dispersion depends on pair separation. For the CDM models presented in this paper, this gives $\langle v^2\rangle^{1/2}_{\rm SCDM} = 675$km/s and $\langle v^2\rangle^{1/2}_{\Lambda\rm CDM} = 590$ km/s, in good agreement with the values measured in the simulations (e.g. Mo, Jing & Börner 1997; Sheth & Diaferio 2000). Because our models allow us to compute this single particle dispersion at any times, they provide a simple way of computing the evolution of the density weighted temperature of the Universe.

4 THE MEAN STREAMING VELOCITY

The scale dependence of the mean streaming $v_{12}(r)$ of dark matter particles has been understood for some time now. Hamilton et al. (1991) showed that because they could provide good estimates of the evolution of $\xi(r,a)$, for any initial correlation function, they could also describe the shape of $v_{12}(r)$ (also see Nityananda & Padmanabhan 1994). Because the halo model presented in the previous section allows one to compute $\xi(r,a)$, by following the steps outlined by Hamilton et al., it can also be used to compute $v_{12}(r)$. We will not do this here. Rather, we will show that because our halo model allows one to split the correlation function up into linear and nonlinear parts, we are able to compute a good approximation to $v_{12}(r)$ rather more simply. Recently, Juszkiewicz, Springel & Durrer (1999) have presented a fitting formula for this statistic; they argue that their formula is simpler to use than the exact method of Hamilton et al. The results presented in this section can be thought of as

providing a simple physical reason for the values of the coefficients in their fitting formula.

The relevant starting point is the pair conservation equation in Peebles' book (Peebles 1980):

$$a\,\frac{\partial(1+\bar{\xi})}{\partial a} = -\frac{v_{12}(r)}{Hr}\;3\left[1+\xi(r)\right], \qquad (14)$$

where $\bar{\xi}(r,a)$ is the volume averaged correlation function on comoving scale $x = r/a$ at the time when the expansion factor is a, and the Hubble constant is H. Note that the partial derivative with respect to a on the left hand side keeps x fixed rather than r. This says that if we know the correlation function for all scales x and all times a, then we can compute how $v_{12}(r)$ depends on scale today; basically it comes from assuming that the number of pairs is conserved. Hamilton et al. also showed that by inserting their expression for the evolution of $\xi(r,a)$ into equation (14) above, they were able to describe $v_{12}(r)$ accurately.

A simpler analytic approach follows from reading through Peebles' logic further. He notes that an approximate solution to equation (14) can be got by assuming that $\bar{\xi}$ evolves according to linear theory: $\bar{\xi}(r = ax, a) = [D(a)/D(a_0)]^2\bar{\xi}(r = a_0x, a_0)$, where $D(a)$ is the linear theory growth factor. Then the left hand side is $a\,\partial\bar{\xi}(ax,a)/\partial a = 2f(\Omega)\,\bar{\xi}(ax,a)$, where $f(\Omega) \equiv \partial\ln D/\partial\ln a \approx \Omega^{0.6}$. So, in this approximation we get

$$-\frac{v_{12}}{Hr} = \frac{2}{3}\frac{f(\Omega)\,\bar{\xi}(r,a)}{1+\xi(r,a)} \qquad (15)$$

This is just the usual linear theory expression with an extra factor of $(1+\xi)$ in the denominator. Juszkiewicz et al. (1999) show that, while this approximation is fine on large scales, it underestimates the exact solution by a factor of 3/2 or so on smaller scales. They use perturbation theory to motivate the introduction of the extra terms they must add to this expression to rectify this problem.

Our model provides another simple way to see what these terms should be. Since the previous section allows us to write ξ as a sum of two terms, we can work out how each one scales with time. In our model, the term which dominates on small scales evolves both because the mass function evolves, and because the concentrations of haloes of a fixed mass depend on when they formed. The term which dominates on larger scales is very similar to that predicted by linear theory. If we assume that it evolves according to linear theory, then

$$-\frac{v_{12}}{Hr} = \frac{1}{3[1+\xi(r,a)]}\left[2f(\Omega)\bar{\xi}_{\rm 2halo}(r,a) + \frac{\partial\bar{\xi}_{\rm 1halo}}{\partial\ln a}\right], \qquad (16)$$

where the derivative of $\xi_{\rm 1halo}$ with respect to expansion factor a can be evaluated because the dependence of the mass function $n(m,a)$ and the halo profiles and their convolutions $\lambda(r|m)$ on a are all known. Thus, we have

$$\begin{aligned}\frac{\partial\bar{\xi}_{\rm 1halo}}{\partial\ln a} &= \frac{\partial\ln m_*}{\partial\ln a}\left[\bar{\xi}_{\rm 1halo}(r,a) - \xi_{\rm 1halo}(r,a)\right] \\ &\quad + \frac{3}{r^3}\int_0^r {\rm d}r'\,r'^2\int_0^\infty {\rm d}m\frac{n(m)}{\bar{\rho}} \\ &\quad \times \frac{\lambda(r|m)}{\bar{\rho}}\frac{\partial\ln\lambda}{\partial\ln c}\,\frac{\partial\ln c}{\partial\ln a}\Big|_{\frac{m}{m_*}}. \end{aligned} \qquad (17)$$

Here c denotes the inverse of the core radius relation of the halo profile (so $c_{\rm NFW} = 1/a_{\rm NFW}$) to avoid confusing the core-radius relation with the cosmological expansion factor. The notation $\partial\ln c/\partial\ln a|_{m/m_*}$ denotes a derivative with respect to $\ln a$ keeping m/m_* fixed. If the time dependence of c comes only from its dependence on m_*, then the final term on the right hand side vanishes, making the expression particularly simple. If, in addition, the correlation function was a pure power-law of slope, say, γ, then $\xi = (3-\gamma)\bar{\xi}/3$. In this case, the term in square brackets in the expression above would become $(\gamma/3)\,\bar{\xi}_{\rm 1halo}$.

To illustrate how the one-halo term scales, it is convenient to study a spectrum with shape $P(k) \propto k^n$ initially. In this case $\partial\ln m_*/\partial\ln a = f(\Omega)\,6/(3+n)$. On very small scales, $\xi \approx \xi_{\rm 1halo}$ is expected to be a power law of slope $\gamma_{\rm SC} \approx 3(3+n)/(5+n)$ (e.g. Peebles 1980). This makes the right hand side of equation (17) equal to $f(\Omega)\,6/(5+n)$ times $\bar{\xi}_{\rm 1halo}$. This is the same as the scaling required by stable clustering (e.g. Hamilton et al. 1991). On intermediate scales, Padmanabhan (1996) argues that $\bar{\xi}$ should be approximately a power-law of slope $\gamma_{\rm QL} \approx 3(3+n)/(4+n)$. If we still set $1+\bar{\xi} \approx \bar{\xi}_{\rm 1halo}$, then the right hand side of equation (17) becomes $f(\Omega)\,6/(4+n)$ times $\bar{\xi}_{\rm 1halo}$. This is precisely the quasi-linear scaling assumed by Padmanabhan (1996). On large scales $\bar{\xi}$ has slope $\gamma_{\rm L} = (3+n)$, and so the right hand side of equation (17) becomes $2\,f(\Omega)\,\bar{\xi}_{\rm 1halo}$, which is the same as the scaling required by linear theory. Thus, our halo profile term (equation 17) interpolates smoothly between these different regimes. Of course, because $\xi_{\rm 1halo}(r)$ is not really a power law, it never actually obeys these scalings exactly. Hamilton et al. (1991) assumed that v_{12} could be written as a function of $\bar{\xi}$ alone. Because our one-halo term actually depends both on $\bar{\xi}_{\rm 1halo}$ as well as on $\xi_{\rm 1halo}$, our halo models are formally inconsistent with the Hamilton et al. ansatz. For example, the ansatz is based on an assumption that clustering on small scales is stable, whereas our halo models are not. Ma & Fry (2000) explore some consequences of this.

Fig. 2 shows that our model,

$$\begin{aligned}-\frac{v_{12}}{Hr} &= \frac{f(\Omega)}{3[1+\xi(r,a)]}\Bigg[2\bar{\xi}_{\rm 2halo}(r,a) + \\ &\qquad \frac{6}{3+n_*}\left[\bar{\xi}_{\rm 1halo}(r,a) - \xi_{\rm 1halo}(r,a)\right]\Bigg]. \end{aligned} \qquad (18)$$

where $n_* = -1.33, -1.53$ is the slope of the power spectrum on the scale m_* for the SCDM and ΛCDM models we consider in this paper, is quite accurate. The triangles show measurements from the publically available Virgo simulations (Jenkins et al. 1998), and crosses show the fitting formula which Juszkiewicz et al. (1999) obtained by fitting to these simulations. The open circles in the panel on the right show the streaming motions in the ΛCDM GIF simulation (e.g. Kauffmann et al. 1999). The GIF SCDM box is only 85 Mpc/h on a side. As a result, the velocities in it are strongly affected by the finite size of the box (Sheth & Diaferio 2000), which is why we have not shown v_{12} from this simulation. The solid curve shows our model (equation 16) which accounts for the fact that evolution on small scales is nonlinear, and weights by the relative fractions of linear and nonlinear pairs. It is the sum of two terms; these are shown as the two dashed curves. Using the linear theory correla-

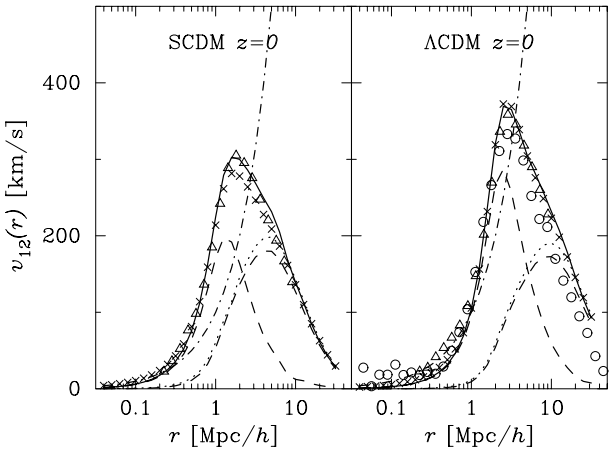

Figure 2. The mean streaming velocity of dark matter particles. Triangles show the Virgo simulation measurements, circles show the GIF ΛCDM simulation, and dot-dashed curves show the Hubble expansion velocity. Crosses show the result of using the Peacock & Dodds (1996) formulae for the correlation function in the fitting formula provided by Juszkiewicz et al. (1999). Solid curves show the model described in the text which accounts for the fact that the nonlinear evolution is different from what linear theory predicts, and then weights the linear and nonlinear scalings by the relative fractions of linear and nonlinear pairs. Dashed curves show the two contributions to the streaming motion in our model; the curves which peak at large r are for pairs in two different haloes. Dotted curve shows the approximation of using the linear theory correlation function to model this two-halo term.

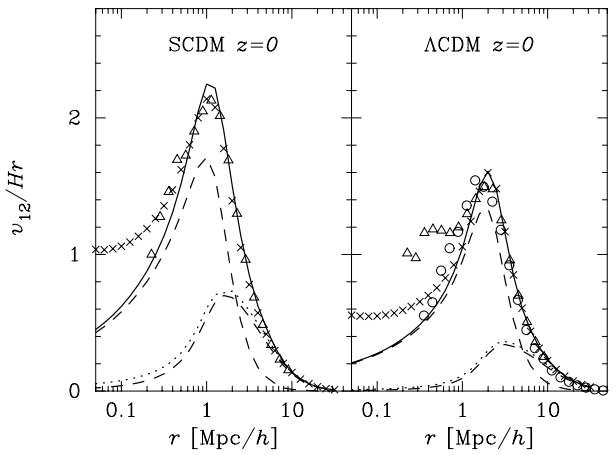

Figure 3. The ratio of the mean streaming velocity of dark matter particle pairs separated by r, to the Hubble expansion on that scale. As in the previous Figure, triangles show the Virgo simulations, circles show the ΛCDM GIF simulation, crosses show the Juszkiewicz et al. (1999) fitting formula, and solid curves, which are the sum of the dashed curves, show our model predictions.

tion function (the dotted curve in the previous figure) to model the contribution from the two-halo term (the dashed curve which dominated on large scales in the previous figure) corresponds to setting $\bar{\xi}_{\rm 2halo} \to \bar{\xi}_0$. This approximation is shown as the dotted curves. The dot-dashed curves show the Hubble expansion velocity for comparison.

To study the approach to stable clustering, it is more useful to show the ratio of the streaming velocity to the Hubble expansion. Recall that one might have expected the smallest scales to have $-v_{12}/Hr = 1$. This follows from the simple scalings we discussed earlier (assuming $\Omega_0 = 1$): set $\bar{\xi}_{\rm 1halo} = 3\xi_{\rm 1halo}/(3-\gamma_{\rm SC})$, and use the fact that $1+\xi \approx \xi_{\rm 1halo}$. Fig. 3 shows that on small scales the mean streaming motions in our halo models are smaller than the stable clustering limit. The streaming motions do not cancel the Hubble expansion. As before, the triangles in the two panels show the Virgo simulations, the crosses show the fitting formula to these simulations, and circles in the panel on the right show the streaming motions in the ΛCDM GIF simulation. Although our model v_{12} curves (solid lines) fall below the stable clustering limit, they are in quite good agreement with the simulations.

Notice that, on scales slightly smaller than a Mpc/h or so, the one-halo term in our models can exceed the Hubble velocity. This shows explicitly that, even if clustering were to approach the stable clustering limit, it would have to do so on scales which are smaller than the virial radii of haloes. This is consistent with arguments in Sheth & Jain (1997). Another way of saying this is that, if $-v_{12}$ equalled Hr out to the virial radii of all haloes, then the one-halo contribution to the mean streaming velocity would be $\xi_{\rm 1halo}/(1+\xi)$: this would give a curve which decreased monotonically from unity as r increased, whereas our one-halo term actually has a peak at $\sim$ 1Mpc/h. On these slightly larger scales, writing our previous scalings for power-law profiles in terms of ξ with slope $\gamma_{\rm QL}$ shows that $-v_{12}/Hr = 2f(\Omega)$. This value is in reasonable agreement with the height of the peak of the solid curve in both panels of Fig. 3. Higher resolution simulations are required to determine whether clustering is stable on scales smaller than about 0.1Mpc/h.

The careful reader will have noticed that our halo models slightly overestimate the amplitude of the streaming motions on large scales. Some of this effect may be due to our simple treatment of $\xi_{\rm 2halo}$. If we were to set $\xi_{\rm 2halo} \to \xi_0$ we would overestimate the true value even more (the dotted curves are always above the dashed ones). However, notice that the single-halo contribution to v_{12} is nonzero even at separations larger than 10Mpc/h, and that it approximately accounts for the overestimate on these scales. Where does this large scale single-halo contribution come from? It does not arise from particles which are falling towards each other from opposite sides of a few proud monster haloes! (A virialized halo with a radius of 5 Mpc/h would have a mass of about $2.5\Omega \times 10^{16} M_\odot/h$.) Rather, at least some of the overestimate of v_{12} arises from the fact that, formally, the halo models violate the integral constraint. As mentioned earlier, the integral of the halo model correlation function over all separations does not equal zero. This means that the model overpredicts the value of the true $\bar{\xi}_{\rm 1halo}$. A glance at Fig. 1 shows that $\xi_{\rm 1halo}$ on the scale of 5 Mpc/h is negligible. This in equation (17) shows that, on these scales, the single-halo contribution to v_{12} is determined almost entirely by the volume average term, and this results in an overestimate.

One way of remedying this is to make the halo profiles compensated, say, by embedding them in slight underdensities. This would have the effect of making the large scale value of $\xi_{\rm 1halo}$ go slightly negative, with a more dramatic effect on large scale values of the volume average $\bar{\xi}_{\rm 1halo}$. While compensated profiles may be physically reasonable, and are certainly of formal interest, we have not pursued this fur-

ther, because the large scales where the spurious streaming velocities appear are also those where the two-halo term dominates the pair statistics.

Before we move on to the second moment of the pairwise velocity distribution, we think it is useful to rewrite our expression for the mean streaming motions one final time. If we use the fact that $\bar{\xi}_{\rm 2halo} \approx \bar{\xi}_0$, then

$$-\frac{v_{12}}{Hr} \approx -\frac{v_{12}^{\rm Lin}}{Hr}\,\frac{1+\xi_0(r)}{1+\xi(r)} + \frac{2f(\Omega)}{3+n_*}\left[\frac{\bar{\xi}_{\rm 1halo}(r)}{\xi_{\rm 1halo}(r)} - 1\right]\frac{\xi_{\rm 1halo}(r)}{1+\xi(r)}, \qquad (19)$$

where we have omitted writing factors of a throughout for brevity, and we have defined $-v_{12}^{\rm Lin}/Hr \equiv 2\bar{\xi}_0/3[1+\xi_0]$, which can be written entirely in terms of linear theory quantities. The factors $\xi_{\rm 1halo}/[1+\xi]$ and $[1+\xi_0]/[1+\xi]$ are simply the fractions of pairs from particles in the same halo, and in separate haloes, respectively. This form shows clearly that the streaming motions arise from applying linear theory to the pairs in separate haloes, nonlinear theory to the pairs in the same halo, and weighting by the fraction of pairs of each type. For instance, stable clustering would yield unity times the nonlinear pair-weight term, and the quasi-linear scaling described above would yield two times the nonlinear pair-weight term. It is this sort of decomposition into linear and nonlinear parts which we will exploit in what follows.

5 THE PAIRWISE VELOCITY DISPERSION

This section provides a simple model of how and why the pairwise velocity distribution depends on scale. The model constructed here is a natural generalization of that studied by Sheth (1996), Diaferio & Geller (1996), and Sheth & Diaferio (2000). It is much simpler than the exact 'cosmic virial theorem' approach (Peebles 1980; Bartlett & Blanchard 1995; Mo, Jing & Börner 1997) one is led to if one attempts to climb the rungs of the BBGKY hierarchy, one-by-one.

5.1 The model assumptions

Let $u(r_{12})$ denote the difference between the velocities of two particles separated by r_{12}, along their line of separation. If the velocities of the particles separated by r_{12} are independent of each other, then the shape of this distribution can be computed from knowledge of the shape of the single particle distribution function directly. On small scales, this assumption of independence is almost certainly wrong. However, in the small separation limit, progress can be made by assuming that all pairs at a given small r_{12} are in the same halo. Since haloes are virialized, particle velocities within a halo are drawn from independent Maxwellian distributions, and so velocity differences are also Maxwellian, albeit with twice the dispersion of the single particle case. The dispersion of the Maxwellian depends on the mass of the parent halo in which the pair is, and so the full distribution of $u(r_{12})$ can be computed by integrating over the distribution of halo masses, weighting by the number of pairs which have separations r_{12} within each halo of mass m. This model is studied in detail in Sheth (1996) and Diaferio & Geller (1996). Of course, their model only applies on scales where, for most pairs, both members are in the same halo.

What happens at larger separations? In this subsection we will study the limit in which both members of the pair are in different haloes. We will argue that, in this limit, the distribution of u is also relatively simple.

As for the correlation function, we begin by writing the dispersion $\sigma_{12}^2(r) = \langle u^2(r)\rangle$ at separation r as the sum of two terms:

$$\sigma_{12}^2(r) = \sigma_{\rm 1halo}^2(r) + \sigma_{\rm 2halo}^2(r), \qquad (20)$$

where the first term arises from pairs in which both members are in the same halo (so it depends on properties of virialized haloes and dominates on small scales), and the second term is for pairs in different haloes (so it dominates on large scales).

As mentioned above, the first term depends on the density profiles of virialized haloes. There are two reasons why it is a function of scale. First, the velocity dispersion within a halo may depend on position within it, so the pairwise dispersion will depend on separation. However, the pairwise dispersion will depend on scale even if we neglect this dependence. To see why, note that we should get a reasonable estimate of this term by setting the dispersion equal to the circular velocity at the outside edge of the halo: $Gm/r_{\rm vir}$ (this would be exact for an isothermal sphere, but is only approximate otherwise), and using this for all $r \le r_{\rm vir}$. In this case,

$$\sigma_{\rm 1halo}^2(r) = \frac{1}{1+\xi(r)}\int {\rm d}m\,\frac{Gm}{r_{\rm vir}}\,\frac{n(m)}{\bar{\rho}}\,\frac{\lambda(r|m)}{\bar{\rho}}. \qquad (21)$$

This expression is exactly like the one in Sheth (1996), except that we have multiplied it by an additional factor of $\lambda(r|m)/[1+\xi(r)]$ to account for the fact that only a fraction of the pairs at a given separation r are in the same m-halo.

To see that this is the correct pair weighting factor, let $U(1,2)\,{\rm d}v_1{\rm d}v_2$ denote the probability that there exists a particle in a cell of size dv_1 within a halo of mass m, and another particle in a cell of size dv_2 which is not necessarily in the same halo. Similarly, let $P(1,2|m)\,{\rm d}v_1{\rm d}v_2$ denote the probability that there exists a particle in a cell of size dv_1 within a halo of mass m, and that the other particle in dv_2 is within the same halo. If each particle carries a mass m_p, then $U = (\bar{\rho}/m_p){\rm d}v_1(\bar{\rho}/m_p)\,[1+\xi(r)]\,{\rm d}v_2$, and $P = mn(m){\rm d}m\,{\rm d}v_1/m_p\,[\lambda(r|m)/m]\,{\rm d}v_2/m_p$. The ratio is the fraction of pairs at separation r which are both in the same m-halo: $P/U = {\rm d}m\,n(m)\lambda(r|m)/(\bar{\rho}/m_p)^2[1+\xi(r)]$. This is the weighting we used in the equation above. Note that this is consistent with equation (7): one plus the left hand side of that expression is the total number of pairs at separation r, and the first term on the right hand side is the contribution from pairs in which both particles were in the same halo. It is also the weighting associated with our final expression for the mean streaming motions (equation 19).

Allowing the dispersion to depend on position in the halo means that

$$\frac{Gm}{r_{\rm vir}}\,\lambda(r|m) \rightarrow 2\pi\int {\rm d}x_1\; x_1^2\,\rho(x_1|m)\int_{-1}^{1}{\rm d}\beta\,\rho(x_2|m) \times \Big[\sigma_{\rm 1d}^2(x_1|m) + \sigma_{\rm 1d}^2(x_2|m)\Big], \qquad (22)$$

where $x_2^2 = x_1^2 + r^2 - 2x_1r\beta$, and where the one dimensional

dispersion, $\sigma^2_{\rm 1d}$, can be approximated by, say, the radial velocity dispersion given in Appendix A.

This shows that at small separations, $\sigma^2_{\rm 1halo}(r)$ increases with r because virial motions within haloes increase as $m^{2/3}$, and only massive haloes can contribute pairs at moderately large separations (there will be an additional scale dependence if we also included the dependence of the dispersion on position within the halo). Therefore the pairwise dispersion will increase with increasing scale at small r. On larger scales, however, an increasing fraction of pairs are actually from different haloes. Since $\lambda(r|m) \to 0$ as r increases, on scales larger than that of a typical halo, $\sigma^2_{\rm 1halo}(r)$ will eventually decrease.

The term in which particles are in different haloes is

$$\sigma^2_{\rm 2halo}(r) = \int\int {\rm d}m_1 {\rm d}m_2 \frac{1+\xi(m_1,m_2|r)}{[1+\xi(r)]} \times \frac{m_1 n(m_1)}{\bar\rho}\,\frac{m_2 n(m_2)}{\bar\rho}\, S(m_1,m_2|r), \quad (23)$$

where $n(m)$ is the number density of m-haloes,

$$\xi(m_1,m_2|r) = b(m_1)b(m_1)\,\xi_0(r) \quad (24)$$

is the correlation function of haloes, $b(m)$ is the linear bias factor discussed earlier, $\xi(r)$ is the correlation function of the mass, and $S(m_1,m_2|r)$ represents the dispersion of the velocity difference along the line of separation between particles separated by r that are in different haloes (one of mass m_1 and the other m_2). Whereas the other terms are simply the pair-weighting, the physics is in finding a convenient expression for S.

If $\sigma^2(m)$ denotes the dispersion associated with a single halo, then

$$S(m_1,m_2|r) = \sigma^2(m_1) + \sigma^2(m_2) - 2\Psi(m_1,m_2|r), \quad (25)$$

where $\Psi(m_1,m_2|r)$ represents the fact that the motion of a particle in halo m_1 may be correlated with that of the particle a distance r away in the halo m_2. Later in this paper we will develop a model for the velocity correlation function. For the time being, we think it clearer to study a simpler case first—in what follows, we will neglect the fact that halo velocities may be correlated.

Before we do so, notice that if haloes were spatially uncorrelated as well, then the pairwise distribution would be the difference of two random variates, so it would be a simple convolution of the single particle distribution derived by Sheth & Diaferio (2000). In what follows, we will study what happens if we account for the fact that haloes are spatially correlated, even though we neglect the fact that their velocities are also correlated.

5.2 Neglecting velocity correlations

Suppose we wish to compute the one-dimensional relative pairwise velocity dispersion along the line of separation. Since we are ignoring velocity correlations, the shape of the pairwise velocity distribution arises from applying the appropriate pair-weight as a function of separation, and integrating over the distribution of dispersions given by the halo mass function (equation (23) with $\Psi = 0$).

The pair-weighting involves the bias factor which depends on halo mass and on the shape of $n(m)$; since we are using the mass function given in Sheth & Tormen (1999), we will use their formula for $b(m)$ also. Let $\langle v^2\rangle$ denote the single particle velocity dispersion (section 3 showed that it has contributions from the virial motions within haloes as well as from the motions of the haloes themselves). Then the bias weighting means that we must compute $2\,\langle b\,v^2\rangle$. Thus, we arrive at a simple expression for the scale dependence of this second term:

$$\sigma^2_{\rm 2halo}(r) = \frac{2}{3}\,\langle v^2\rangle\,\frac{1+\xi_0(r)\langle b\,v^2\rangle/\langle v^2\rangle}{1+\xi(r)}, \quad (26)$$

where $\langle v^2\rangle$ is the three dimensional dispersion given by the cosmic energy equation. The factor of 2/3 arises because we are interested in the sum of two (assumed independent) velocity variates, and we are only interested in one of the three velocity components.

At large separations $\xi(r) \approx \xi_0(r)$, and they are both $\ll 1$, so $\sigma^2_{\rm 2halo} \to 2\,\langle v^2\rangle/3$, as one expects for independent variates. What about intermediate separations? In this model, $\sigma^2_{\rm 2halo}(r)$ depends on scale primarily because $\xi(r)$ does. On intermediate scales (where the assumption that the velocities are independent is certainly wrong!), whether or not $\sigma^2_{\rm 2halo}$ increases or decreases with scale depends on the ratio $\langle b\,v^2\rangle/\langle v^2\rangle$. For example, the weighting by b increases the contribution from massive haloes relative to less massive ones. Since virial motions within massive haloes generate velocities that are larger than the rms, for the dark matter, this ratio is likely to be larger than unity. This means that $\sigma^2_{\rm 2halo}$ may be slightly higher on intermediate scales than on large ones. On small scales, the pair-weighting term $\xi_0/(1+\xi)$ decreases rapidly, so $\sigma^2_{\rm 2halo}$ will also decrease.

Fig. 4 compares our simple model with what is measured in simulations. Circles show the GIF simulation results, and triangles show the VIRGO simulation results of

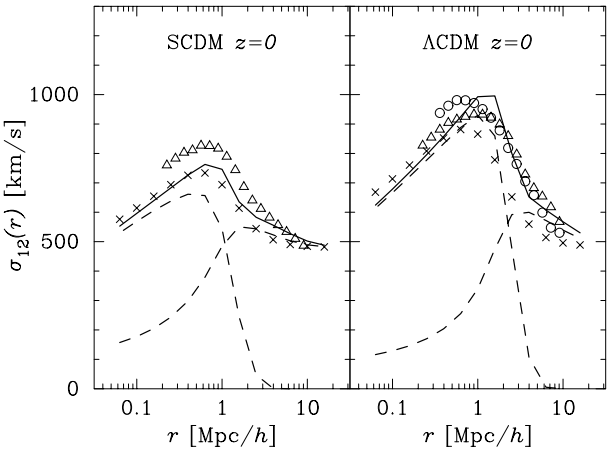

Figure 4. Scale dependence of the pairwise velocity dispersion. Triangles show the Virgo simulation results of Jenkins et al. (1998), circles show the GIF simulation results, and crosses show the fitting formula for the dark matter provided by Mo, Jing & Börner (1997). Solid curves show the scale dependence in our model which neglects the spatial dependence of the dispersion within a halo, and also neglects velocity correlations between haloes, but includes the effects of spatial correlations. Dashed curves show the contribution from pairs in which both particles are in the same halo (hence the peak at small r) and in separate haloes (so a peak at large r), respectively.

Jenkins et al. (1998). Crosses show a fitting function, equation (40) of Mo, Jing & Börner (1997), which should describe the scale dependence of the pairwise dispersion. In all cases, we have chosen to follow standard practice and not centre the statistic: to centre, the mean streaming motion v_{12} should be subtracted in quadrature.

Although the GIF and Virgo simulation results are in reasonable agreement on large scales, $\sigma_{12}^{\rm GIF}$ is larger, by about 100 km/s, on scales smaller than a Megaparsec or so. Presumably, this difference arises from the fact that, although the two simulations used the same number of particles, the boxes had different sizes and the particle masses were also different. The Virgo boxes had sides of length $L = 240{\rm Mpc}/h$, the GIF ΛCDM box was 141 Mpc/h. The finite box size has two effects: first, large scale flows have smaller amplitudes in small boxes, and so this affects the large-scale value of the pairwise dispersion. In addition, small boxes do not have a fair sample of the massive haloes which dominate the pairwise velocity statistic at a Megaparsec. Because massive haloes are rare, the pairwise statistic will have a large scatter; the large value of σ_{12} we measured in the smaller GIF simulation may simply be a large fluctuation. On the other hand, because of its better mass resolution, the GIF box is able to resolve substructure within virialized haloes which the Virgo simulations can not. The presence of substructure will increase the velocity dispersion. However, because this contribution only adds in quadrature, it is not clear that this can account for all the difference.

We have tried to incorporate the effect of the finite box size into our model by restricting our integrals over halo masses to the range $m < 10^{16} M_\odot/h$, and by only integrating over $k > 2\pi/L$ when using the cosmic energy equation to estimate $\langle v^2\rangle$. The dashed curves show the two types of terms in our model after setting the box size to $L = 141{\rm Mpc}/h$. We chose to model the smaller box because the GIF semianalytic galaxy formation models of Kauffmann et al. (1999), which we will use later in this paper, use this same simulation. The dashed curve which peaks at small r is for pairs in which both particles are in the same halo, and the dashed curve which peaks at large r is for particles in different haloes. The solid curve is the sum (in quadrature) of the two contributions, plus a piece which comes from the fact that the statistic is not centred (see below). Our model appears to describe the main features of $\sigma_{12}(r)$ reasonably well.

On small scales, discrepancies between the model and simulations are not caused by our neglect of the halo velocity correlation function; this regime is dominated by pairs which are in the same halo, which suggests that it is the assumption that the pairwise dispersion within haloes is isotropic and independent of position within the halo, as it would for an isothermal sphere, which should be changed. If one is willing to assume the orbits within the halo are isotropic, then this can be done by using the expressions for the radial velocity dispersion we provide in Appendix A. We will show the results of doing this in the next subsection.

On large scales, the difference between the symbols and the solid curve is a measure of the importance of velocity correlations. The relatively good agreement on larger scales suggests that our neglect of the halo velocity correlation function is not a bad approximation. We think it remarkable that we are able to provide a reasonably accurate description of the rise and fall of the pairwise velocity dispersion without once mentioning the three-point correlation function.

5.3 Including velocity correlations

This subsection shows how one might include the effects of correlated velocities. To do so, we briefly summarize the results of Sheth & Diaferio (2000). They argued that in a model in which all particles are in haloes, such as the one we are studying in this paper, it is sensible to write a particle's velocity as the sum of two terms:

$$v = v_{\rm vir} + v_{\rm halo}, \qquad (27)$$

where $v_{\rm vir}$ is the virial motion of the particle about the halo centre of mass, and $v_{\rm halo}$ is the motion of the parent halo. Let $\sigma^2(m)$ denote the dispersion of particle velocities in m-haloes. It can be written as the sum of the two terms: $\sigma^2_{\rm vir}(m) + \sigma^2_{\rm halo}(m)$. Sheth & Diaferio showed that $\sigma^2_{\rm vir} \propto Gm/r_{\rm vir}$, and that (appropriately smoothed) linear peak theory (Bardeen et al. 1986) could be used to estimate $\sigma^2_{\rm halo}(m)$ at any given time rather accurately. Namely, $\sigma_{\rm halo}(m) \approx H\Omega^{0.6}\sigma_{-1}(m)\,C(m)$, where σ_{-1} is computed by multiplying $P(k)$ with a smoothing filter $W[kR(m)]$ of scale $R(m)$, integrating over k, and dividing by $2\pi^2$, and $C(m)$ is a correction factor which accounts for the fact that peaks have slightly lower rms velocities than random patches (see Sheth & Diaferio for the exact expressions).

In such a model, virial motions are random: the virial velocity of a particle is not correlated with the motion of the other particles in the halo, nor with the value of $v_{\rm halo}$, nor with the motion of any other particle in any other halo. This means that correlated motions arise because halo motions may be correlated, and not otherwise. If the virial velocity is independent of pair separation r, then $\Psi(m_1, m_2|r)$ in equation (25) represents the correlations of halo motions for m_1 and m_2-haloes separated by r. Strictly speaking, a range of halo separations can contribute to the same particle separation r, but we are ignoring that here, just as we did when computing the correlation function.

Since linear theory predicts how the velocity correlation function depends on smoothing scale (Górski 1988), and since linear theory provides a reasonably good description of the rms motions of haloes (Sheth & Diaferio 2000), it is relatively straightforward to include the linear theory correlations in our model. The final term comes from the fact that the statistic is not centred.

We will approximate the velocity correlation as follows. Suppose for the time being that ignoring the peak constraint gave a reasonable approximation to halo velocities. Then $\sigma_{\rm halo}(m) \approx H\Omega^{0.6}\sigma_{-1}(m)$. Similarly, the correlation in velocity between patches of different sizes, say $R(m_1)$ and $R(m_2)$, along the line of their separation, is

$$\psi(m_1, m_2|r) \equiv H^2\Omega^{1.2}\int\frac{{\rm d}k}{2\pi^2}P(k)\,W(k|m_1, m_2)\,K(kr), \qquad (28)$$

where

$$W(k|m_1, m_2) \equiv W[kR(m_1)]\,W[kR(m_2)],$$

and the Ws are the Fourier transforms of tophat window functions, and

$$K(x) = \frac{\sin x}{x} - \frac{2}{x^3}(\sin x - x\cos x).$$

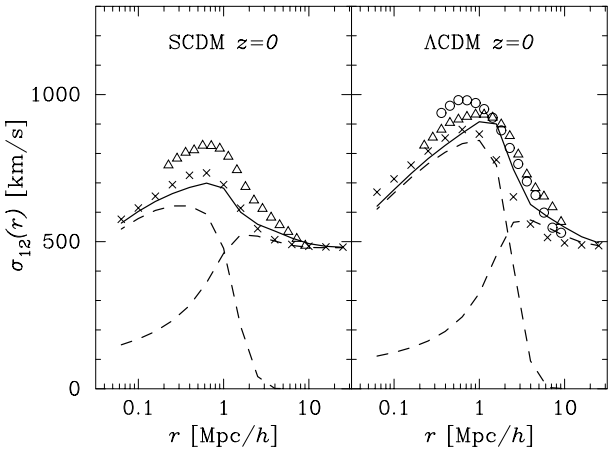

Figure 5. Scale dependence of the pairwise velocity dispersion. Symbols, the same as in the previous figure, represent the simulation results. Solid curves show the scale dependence in our model after including the fact that the dispersion within a halo depends on position within the halo, and also accounting crudely for the effects of spatial as well as velocity correlations. The two dashed curves show the contribution from pairs in which both particles are in the same halo (peak at small r) and in separate haloes (peak at large r).

This generalizes the expression in Górski (1988), which assumed $R(m_1) = R(m_2)$. A simple way to include the peak constraint, at least approximately, is to multiply by the appropriate peak constraint factors:

$$\Psi(m_1, m_2|r) \approx \frac{\sigma_{\rm halo}(m_1)}{\sigma_{-1}(m_1)} \frac{\sigma_{\rm halo}(m_2)}{\sigma_{-1}(m_2)} \psi(m_1, m_2|r). \qquad (29)$$

This includes the fact that peaks have lower rms velocities than random patches, but assumes that the correlations are otherwise unchanged.

At first sight, inserting this correlation term into equation (23) appears to involve a triple integral—one over m_1, one over m_2, and one over k. In practice, it is much more efficient to rearrange the order of the integrals so that the integral over k is done last. The integrals over m_1 and m_2 are separable and equal. If we use $\Sigma(k)$ to denote the result of the integral over m of $mn(m)$ times the window function $W[kR(m)]$, and $\Sigma_b(k)$ to denote the integral of $mn(m)\,b(m)\,W[kR(m)]$, then the remaining integral over k is really of the form $\int {\rm d}k\; P(k)\,[\Sigma^2(k) + \Sigma_b^2(k)]\,K(kr)/2\pi^2$. The result of all this is that

$$\begin{aligned} S(m_1, m_2|r) \;=\; & \sigma^2_{\rm vir}(m_1) + \sigma^2_{\rm vir}(m_2) \\ & + \sigma^2_{\rm halo}(m_1) + \sigma^2_{\rm halo}(m_2) - 2\Psi(m_1, m_2|r) \\ & + \frac{b(m_1)\,b(m_2)\;v_{12}^2(r)}{2[1 + b(m_1)\,b(m_2)\xi_0(r)]}, \end{aligned} \qquad (30)$$

where the σs are assumed to be the dispersions in one dimension. The final term comes from the fact that the statistic is not centred. It was obtained by expanding $\langle (v_1 - v_2)^2 (1 + b_1\delta_1)(1 + b_2\delta_2)\rangle$ in δ_1 and δ_2, and using the linear theory relation between v and δ (e.g. Fisher 1995).

Fig. 5 compares our model with what is measured in simulations. The symbols are the same as in the previous figure; they are included to show the uncertainties associated with the measurements to date, and the influence of the finite size of the simulation box. As before, we have accounted for the finite box size (which we set to $L = 141$ Mpc/h) when showing our model predictions. The two dashed curves are the model predictions for pairs in which both particles are in the same halo (peak at small r), and in different haloes (peak at large r). The solid curve is the sum in quadrature of the two contributions, plus a piece which comes from the fact that the statistic is not centred.

In addition to including the effects of velocity correlations (which affects the two-halo term), we have modified the one-halo term to include the fact the velocity dispersion within a halo depends on position within the halo, as described in the Appendix. A glance at Fig. A2 shows that, for massive haloes, the isothermal assumption overestimates the dispersion. Because the peak is mainly due to pairs in massive haloes, using what is, arguably, the more realistic value for the dispersion lowers the height of the peak. With these two changes, our model falls significantly below the SCDM results. In the ΛCDM model, on the other hand, our model appears to be in reasonable agreement with the simulations, though it too underestimates the simulation results, especially on small scales.

5.4 Dependence on trace-particle type

Our model has the virtue that it is straightforward to study how the pairwise velocity dispersion depends on the type of trace particle. For example, if only haloes were used to construct this statistic, one would expect the large scale asymptotic value of σ_{12} to be smaller than for the dark matter, since, in this case, the virial term does not contribute to the dispersion. Figure 1 of Sheth & Diaferio (2000) suggests that the term which remains depends slightly on halo mass, and that linear theory, smoothed on the appropriate scale, provides a reasonably good estimate of what it is.

In addition to being smaller than the dark matter pairwise dispersion, the scale dependence of $\sigma_{12}(r)$ for haloes will also be different than it is for dark matter. We can use the results above to estimate how it scales. For halos, there is no contribution from virial motions, so

$$\begin{aligned} \sigma_{12}^{\rm halos}(r) \;=\; & \iint {\rm d}m_1\,{\rm d}m_2\; \frac{1 + \xi_{\rm hh}(m_1, m_2|r)}{[1 + \Xi_{\rm hh}(r)]} \\ & \times\; n(m_1)\,n(m_2)\,H(m_1, m_2|r) \end{aligned} \qquad (31)$$

where

$$1 + \Xi_{\rm hh} \equiv \iint {\rm d}m_1\,{\rm d}m_2\,n(m_1)\,n(m_2)\Big[1 + \xi_{\rm hh}(m_1, m_2|r)\Big],$$

and $H(m_1, m_2|r)$ is given by equation (30) with the virial terms set to zero. A more exact expression, appropriate for peaks identified with the same smoothing scale ($m_1 = m_2$ in our notation), has been provided by Regös & Szalay (1995): our approximate expression is very similar to their equation (68).

Equation (31) shows that $\sigma_{12}^{\rm halos}$ at intermediate r should be slightly smaller than the asymptotic large r value, whereas the pairwise dispersion is larger at intermediate r for the dark matter.

Galaxies in massive haloes are essentially trace particles, so their motions are similar to the motions of dark matter particles (see Sheth & Diaferio 2000 for some subtleties associated with motions of galaxies in less massive

haloes). For the velocity dispersion statistic, the important difference between galaxies and dark matter particles is that, whereas the number of dark matter particles in a halo is proportional to halo mass, and the number of haloes in a halo is unity (of course!) for all haloes, the number of galaxies in a halo is something in between. Essentially, this happens because the number of galaxies in a halo is proportional not to the total amount of gas in the halo, but to the amount of gas which can cool. So the number of galaxies increases with halo mass, but not as quickly as the number of dark matter particles does. Thus, relative to the statistics of dark matter particles, galaxies downweight the contribution from massive haloes. Since massive haloes have large virial motions, these are less pronounced for galaxies than for dark matter. As a result, the pairwise dispersion of galaxies will be smaller in amplitude, and less scale-dependent, than that of the dark matter. This was first noticed by Jing, Mo & Börner (1998), who pointed out that this is what was required for consistency with observations.

Peacock & Smith (2000) used a simple $N_{\rm gal}(m)$ prescription to generate galaxies from their dark matter simulations. They then measured the pairwise dispersion of the model galaxies in their simulations. Our analytic estimate of the pairwise dispersion of the dark matter allows us to do analytically what Peacock & Smith did numerically. First, we use the $N_{\rm gal}(m)$ relation to compute the correlation function of galaxies. Essentially, this can be done by setting $\rho(r|m) \to \rho(r|m)\,N_{\rm gal}(m)/m$ in Section 2 (but see Seljak 2000, Peacock & Smith 2000, or Scoccimarro et al. 2000 for some subtleties associated with how exactly this is done). We then use this pair-weighting to compute the velocity dispersion of our model galaxies.

Specifically, we set

$$\sigma^2_{\rm g1halo}(r) = \frac{1}{1+\xi_{\rm gal}(r)} \int {\rm d}m \, \frac{Gm}{r_{\rm vir}} \times \frac{\langle N^2_{\rm gal}(m)\rangle}{m^2} \, \frac{n(m)}{\bar{n}_{\rm gal}} \, \frac{\lambda(r|m)}{\bar{n}_{\rm gal}} \quad (32)$$

where $\bar{n}_{\rm gal} \equiv \int {\rm d}m\, mn(m) N_{\rm gal}(m)/m$ and $\xi_{\rm gal}(r)$ is the galaxy correlation function (see e.g. Seljak 2000; Scoccimarro et al. 2000), and

$$\sigma^2_{\rm g2halo}(r) = \int\int {\rm d}m_1 {\rm d}m_2 \, \frac{1+\xi(m_1,m_2|r)}{3\,[1+\xi_{\rm gal}(r)]} \times \left[\frac{N_{\rm gal}(m_1)}{m_1}\right] \left[\frac{N_{\rm gal}(m_2)}{m_2}\right] \times \frac{m_1 n(m_1)}{\bar{n}_{\rm gal}} \, \frac{m_2 n(m_2)}{\bar{n}_{\rm gal}} \, S(m_1,m_2|r), \quad (33)$$

where $S(m_1,m_2|r)$ is as in equation (30).

To illustrate, Fig. 6 shows the result of doing this using the $N_{\rm gal}(m)$ relation obtained from the publically available GIF ΛCDM semi-analytic galaxy formation models of Kauffmann et al. (1999). We actually used the simple fit to this relation, for galaxies brighter than $M_B \le -17.5 + 5\log h$ after correcting for the effects of dust, provided by Sheth & Diaferio (2000). The panel on the left shows the correlation functions of the dark matter (open circles) and the galaxies (stars), and our models for the two correlation functions (solid lines). The bottom left panel shows the square root of the ratio of the two correlation functions.

The open circles in the panel on the right show the mean streaming motions and the pairwise dispersions of the dark matter particles, and the stars show the corresponding statistics for the semianalytic galaxies. We assigned velocities to the galaxies slightly differently than how Kauffmann et al. (1999) did. Namely, for the central galaxy in a halo, and for all haloes in which there was only one galaxy, we used the halo centre of mass velocity, rather than the velocity of the nearest particle to represent the motion of the galaxy. The difference between the two speeds is typically about 80 km/s; this means that our values for the mean streaming and velocity dispersion statistics are slightly smaller than the ones presented in Fig. 13 of Kauffmann et al. (1999).

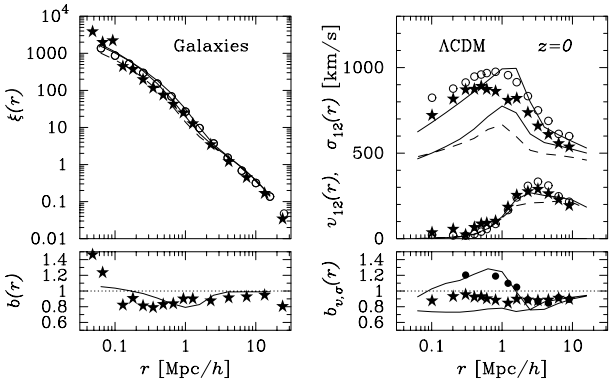

Figure 6. The correlation function and pairwise velocity dispersion for simple models of galaxies. Open circles in both panels show the statistics of the dark matter in the ΛCDM GIF simulation, and stars show the corresponding statistics computed using the semianalytic bright, extinction corrected galaxies of Kauffmann et al. (1999), measured in the same simulation. Solid curves show our model predictions. The two bottom panels show the square root of the ratio of the galaxy and dark matter correlation functions, and the ratio of the streaming motions and rms pairwise velocities, respectively. Dashed curves in the top panels show our model predictions for the semianalytic models of Benson et al. (2000).

The bottom right panel shows the ratio of the mean streaming motions of galaxies to that of the dark matter (filled circles) and the ratio of the rms pairwise velocity of galaxies to that of the dark matter (filled stars). Solid lines show our model predictions. We used the simpler isothermal approximation, rather than the actual position dependent dispersion, when computing the model predictions. Both in the simulations and in our model, the pairwise dispersion for the galaxies falls below that of the dark matter, although our model overestimates the amount by which this happens. The streaming motions of galaxies are similar to those of the dark matter on large scales because the galaxies have a bias factor which is close to unity. Presumably, if the large scale bias factor were different from unity, the streaming motions on large scales would also be different from the dark matter. On small scales, however, the galaxy mean streaming motions can be rather different from that of the dark matter; our model is able to provide quite a good description of this difference.

Benson et al. (2000) showed that the pairwise dispersions of galaxies in their semianalytic galaxy formation models are lower than those of Kauffmann et al. (1999), and that the reason for this was because the two models have different

$N_{\rm gal}(m)$ relations. Therefore, we also looked at a model in which $N_{\rm gal}(m) = (m/10^{12.9}M_\odot/h)^{0.6}$ for haloes more massive than $3\times10^{11}M_\odot/h$; this provides a good fit to the Benson et al. (2000) models with $M_B \le -19.5 + 5\log h$, and is similar to the sort of scaling which Jing, Mo & Börner (1998) argued was required for agreement with observations. The dashed curves in the two upper panels of Fig. 6 show our model predictions when this relation is used. The correlation functions of the two semi-analytic models are similar despite the different brightness cuts. However, because this model has fewer galaxies in massive haloes than the Kauffmann et al. model, the pairwise dispersion of the galaxies in this model is lower. This is because, compared to the correlation function, the pairwise dispersion has an extra $Gm/r_{\rm vir} \propto m^{2/3}$ dependence on halo mass, so it is that much more sensitive to the presence or absence of massive haloes. The Benson et al. models for galaxies with $M_B \le -18.5+5\log h$ are well fit by $N_{\rm gal}(m) = (m/10^{12.6}M_\odot/h)^{0.75}$. If we use this relation instead, then the amplitude of σ_{12} increases. This is consistent with what Benson et al. measured in their simulations.

6 DISCUSSION

Writing the correlation function as the sum of two terms, one which is essentially described by linear theory, and dominates on large scales, and another which is inherently nonlinear, and dominates on small scales, is both accurate and useful. Such a split has been used to model the spatial distribution of the dark matter and of galaxies (Seljak 2000; Peacock & Smith 2000; Scoccimarro et al. 2000). Sheth & Diaferio (2000) show that a similar split can be applied to velocities; particle velocities can also be written as the sum of linear and nonlinear parts. In this paper, we used this split to compute simple estimates not just of the correlation function of dark matter particles, but of the single particle velocity dispersion (the density weighted temperature) and its evolution, and the scale dependence of the first and second moments of the pairwise velocity distribution as well.

Our model provides a good description of the scale dependence of the mean streaming velocities (Figs. 2 and 3). It also provides a reasonably good description of the scale dependence of the pairwise dispersion, provided one restricts attention to scales larger than a Megaparsec or so (Figs. 4 and 5); our model appears to underestimate the value of σ_{12} on scales smaller than 1 Mpc/h. This is, perhaps, surprising, because on these smaller scales, most pairs are in the same halo, and one might have thought that virialized haloes were rather simple to model. Our model assumes that virialized haloes are smooth (or, more importantly, that substructure does not substantially affect the velocity dispersion), and that the velocity dispersion within them is isotropic. The discrepancy between our model and the simulations suggests that one or both of these assumptions is wrong. To model the small separation regime accurately, we may have to resort to using the exact approach based on the BBGKY hierarchy (e.g. Peebles 1980). As we mentioned in the introduction, this approach is considerably more complicated, because it requires knowledge of the three-point correlation function. Although this can be done within the context of these halo models using results presented in Scoccimarro et al. (2000), we have not done so here.

Despite the shortcomings of our model for the pairwise dispersion on small scales, we feel that there are at least two reasons why it is useful. First, it is much simpler than the exact approach one is led to from the BBGKY hierarchy, for which knowledge of the three-point correlation function is required. Secondly, it is easily extended to provide predictions as a function of trace particle type. This is particularly useful for comparing theoretical models with observations of galaxies. Section 5.4 showed how to model the dependence on separation of the galaxy pairwise velocity dispersion.

The main reason for doing this was the following. Our model for the linear and nonlinear contributions to the number of pairs at a given separation can be combined with Sheth & Diaferio's model for the linear and nonlinear contributions to velocities, to model how the full distribution of pairwise velocities (not just the first and second moments) depend on pair separation. Such a model can be extended to describe galaxies, just as we did here. Following Fisher (1995), this allows us to estimate the effect of redshift space distortions on the shape of the galaxy correlation function over the entire range of linear to nonlinear scales. This is the subject of work in progress.

ACKNOWLEDGMENTS

This collaboration was started at the German American Young Scholars Institute in Astroparticle Physics, at the Aspen Center for Physics in the fall of 1998, and at Ringberg Castle in 1999. RKS thanks the IAS, as well as the University and Observatory at Torino, and LH & RS thank Fermilab for hospitality where parts of this work were done. We all thank the Halo Pub for inspiring nourishments. The N-body simulations, halo and galaxy catalogues used in this paper are publically available at `http://www.mpa-garching.mpg.de/NumCos`. The simulations were carried out at the Computer Center of the Max-Planck Society in Garching and at the EPCC in Edinburgh, as part of the Virgo Consortium project. In addition, we would like to thank the Max-Planck Institut für Astrophysik where some of the computing for this work was done. RKS is supported by the DOE and NASA grant NAG 5-7092 at Fermilab. LH is supported by NASA grant NAG5-7047, NSF grant PHY-9513835 and the Taplin Fellowship. He also thanks the DOE for an Outstanding Junior Investigator Award (grant DE-FG02-92-ER40699). RS is supported by endowment funds from the IAS.

REFERENCES

Benson A. J., Baugh C. M., Cole S., Frenk C. S., Lacey C. G., 2000, MNRAS, 311, 793
Davis M., Miller A., White S. D. M., 1997, ApJ, 490, 63
Diaferio A., Geller M., 1996, ApJ, 467, 19
Fisher K. B., 1995, ApJ, 448, 494
Górski K., 1988, ApJ, 332, L7
Hamilton A. J. S., Kumar P., Lu E., Matthews A., 1991, ApJ, 374, L1
Jenkins A., Frenk C. S., Pearce F. R., Thomas P. A., Colberg

J. M., White S. D. M., Couchman H. M. P., Peacock J., A., Efstathiou G., Nelson A. H., 1998, ApJ, 499, 20
Jing Y. P., Mo H. J., Börner G., 1998, ApJ, 494, 1
Juszkiewicz R., Fisher K. B., Szapudi I., 1998, ApJ, 504, L1
Juszkiewicz R., Springel V., Durrer R., 1999, ApJ, 518, L25
Kauffmann G., Colberg J. M., Diaferio A., White S. D. M., 1999, MNRAS, 303, 188
Ma C. P., Fry J., 2000, ApJ, submitted
McClelland J., Silk J., 1977, ApJ, 217, 331
Mo H. J., White S. D. M., 1996, MNRAS, 282, 347
Mo H. J., Jing Y. P., Börner G., 1997, MNRAS, 286, 979
Neyman J., Scott, E. L., 1959, Handbuch Phys., 53, 416
Nityananda R., Padmanabhan T., 1994, MNRAS, 271, 976
Navarro J., Frenk C., White S. D. M., 1997, ApJ, 490, 493
Padmanabhan T., 1996, MNRAS, 278, 29P
Peacock J., Smith R., 2000, MNRAS, submitted, astro-ph/0005010
Peebles P. J. E., 1980, The Large Scale Structure of the Universe. Princeton Univ. Press, Princeton
Press W., Schechter P., 1974, ApJ, 187, 425
Regös E., Szalay A. S., 1995, MNRAS, 272, 447
Seljak U., 2000, MNRAS, in press, astro-ph/0001493
Scoccimarro R., Sheth R. K., Hui L., Jain B., 2000, ApJ, accepted, astro-ph/0006319
Sheth R. K., 1996, MNRAS, 279, 1310
Sheth R. K., Jain B., 1997, MNRAS, 285, 231
Sheth R. K., Lemson G., 1999, MNRAS, 304, 767
Sheth R. K., Tormen G., 1999, MNRAS, 308, 119
Sheth R. K., Diaferio A., 2000, MNRAS, submitted

APPENDIX A: HALO PROFILES

We study a number of different halo profiles below. For each profile, we will be interested in how the density ρ, the circular velocity v_c, the radial velocity dispersion σ_r^2, and the potential ϕ depend on distance from the halo centre. In addition, we will be interested in the convolution of a profile with itself: λ.

The circular velocity at a distance r from the centre of a halo is defined as the square root of the ratio of the mass interior to r and r:

$$v_c^2(r|m) \equiv \frac{G\,m(<r)}{r} = \frac{4\pi G}{r}\int_0^r \mathrm{d}x\; x^2\,\rho(x|m). \qquad \text{(A1)}$$

This, averaged over the profile shape, is

$$mV_c^2(m) \equiv 4\pi \int \mathrm{d}r\; r^2\,\rho(r|m)\,v_c^2(r|m). \qquad \text{(A2)}$$

The potential energy at r is

$$\begin{aligned}\phi(r|m) &= \frac{-4\pi G}{r}\int_0^r \mathrm{d}r'\; r'^2\,\rho(r'|m) \\ &\quad -4\pi G\int_r^\infty \mathrm{d}r'\; r'\,\rho(r'|m). \qquad \text{(A3)}\end{aligned}$$

The total potential energy is this, integrated over the halo:

$$W(m) = 2\pi\int \mathrm{d}r\; r^2\,\rho(r|m)\,\phi(r|m) = -mV_c^2(m), \qquad \text{(A4)}$$

where the final equality follows after rearranging the order of the integrals. If a halo is assumed to be in equilibrium, and the orbits within it are assumed to be isotropic, then the Jeans equation can be used to compute the radial velocity dispersion σ_r^2:

$$-\frac{\mathrm{d}\,\rho\sigma_r^2}{\mathrm{d}r} = \rho(r|m)\,\frac{\mathrm{d}\,\phi}{\mathrm{d}r} = \rho(r|m)\,\frac{Gm(<r)}{r^2}. \qquad \text{(A5)}$$

The total kinetic energy of the halo is

$$K(m) = \frac{3}{2}\,4\pi\int \mathrm{d}r\; r^2\,\rho(r|m)\sigma_r^2(r|m) = \frac{3}{2}\,\frac{mV_c^2(m)}{3}. \qquad \text{(A6)}$$

These relations between W, K and the circular velocity are true for all profiles, and will be a useful consistency check in what follows. Notice that $-W(m) = 2K(m)$: the haloes are in virial equilibrium.

A1 The Hernquist profile

The mass associated with this profile is finite even though the halo extends smoothly to infinity. For this reason, it will be a very useful benchmark calculation in what follows. For a halo of mass m at $r_{\rm vir}$, the profile is

$$\frac{\rho_{\rm H}(s)}{\bar\rho} = \frac{\Delta_{\rm vir}}{3\Omega}\,\frac{2b\,(1+b)^2}{s\,(b+s)^3} = \frac{\Delta_{\rm vir}}{3\Omega}\,\frac{2\,(1+b)^2}{b^3\,x\,(1+x)^3}, \qquad \text{(A7)}$$

where $\Delta_{\rm vir}$ is the average density within $r_{\rm vir}$ in units of the critical density, $s = r/r_{\rm vir}$, b is a core radius in units of $r_{\rm vir}$, and $x = s/b$. The mass interior to r is given by

$$\frac{m(<r)}{m} = \frac{(1+b)^2\,x^2}{(1+x)^2}, \qquad \text{(A8)}$$

the circular velocity is

$$v_c^2(r) = \frac{Gm(<r)}{r} = \frac{Gm}{r_{\rm vir}}\,\frac{x\,(1+b)^2}{b\,(1+x)^2}, \qquad \text{(A9)}$$

and the radial velocity dispersion σ_r^2, which can be computed from the Jeans equation, is also analytic:

$$\begin{aligned}\frac{\sigma_r^2(r)}{Gm/r_{\rm vir}} &= \frac{(1+b)^2}{12b}\Big[12x(1+x)^3\ln\Big(\frac{1+x}{x}\Big) - \\ &\qquad \frac{25x+52x^2+42x^3+12x^4}{1+x}\Big] \qquad \text{(A10)}\end{aligned}$$

(Hernquist 1990; Cole & Lacey 1996). The potential energy at r of such a halo is

$$\phi(r) = -\frac{Gm}{r_{\rm vir}}\,\frac{(1+b)^2}{b(1+x)}, \qquad \text{(A11)}$$

and so the total potential energy of the halo is

$$W_{\rm H} = \frac{4\pi}{2}\int \mathrm{d}r\; r^2\,\rho_{\rm H}(r)\,\phi(r) = -\frac{Gm^2}{6r_{\rm vir}}\,\frac{(1+b)^4}{b} \qquad \text{(A12)}$$

(Hernquist 1990). It is straightforward to verify that the kinetic energy $K_{\rm H} = -W_{\rm H}/2$: the halo is in virial equilibrium. A similar averaging of $v_c^2(r)$ equals $-W_{\rm H}$.

The convolution of such a profile with itself is

$$\frac{4\pi r_{\rm vir}^3\,b^3}{m^2}\,\frac{\lambda_{\rm H}(r|m,b)}{(1+b)^4} = \frac{4}{x^4}\,\frac{h_1(x)-h_2(x)}{(2+x)^4}, \qquad \text{(A13)}$$

where

$$\begin{aligned}h_1(x) &= \frac{24+60x+56x^2+24x^3+6x^4+x^5}{1+x} \quad \text{and} \\ h_2(x) &= \frac{12\,(1+x)\,(2+2x+x^2)\ln(1+x)}{x}.\end{aligned}$$

A little algebra shows that $2\pi G\int \mathrm{d}r\; r\,\lambda_{\rm H}(r|m,b)$ equals the potential energy of the halo, as it should.

A2 The truncated singular isothermal sphere

In this case a halo of mass m is truncated at its virial radius $r_{\rm vir}$. On scales smaller than this,

$$\frac{\rho(r)}{\bar\rho} = \frac{\Delta_{\rm vir}/3\Omega}{s^2}, \qquad \text{(A14)}$$

where $s = r/r_{\rm vir}$, and $\Delta_{\rm vir}$ is a constant which specifies how dense the halo is relative to the critical density at the time: $3m/4\pi r_{\rm vir}^3 = \Delta_{\rm vir}\rho_{\rm crit}$. The circular velocity within the halo is

$$v_{\rm c}^2 = Gm/r_{\rm vir}, \qquad \text{(A15)}$$

and the radial velocity dispersion within the halo is $\sigma_r^2 = v_{\rm c}^2/2$; for an isothermal sphere, $v_{\rm c}$ and σ_r are independent of position within the halo. The convolution of such a profile with itself is

$$\frac{4\pi r_{\rm vir}^3}{m^2}\,\lambda_{\rm Iso}(r|m) = \frac{1}{s}\int_{s/2}^{1}\frac{{\rm d}x}{x}\ln\left|\frac{x}{s-x}\right| \quad \text{if } 0\le s\le 2, \qquad \text{(A16)}$$

and the truncation means that it is zero on separations larger than twice $r_{\rm vir}$. So, for a truncated isothermal sphere

$$2\pi G\int {\rm d}r\; r\,\lambda_{\rm Iso}(r|m,b) = \frac{Gm^2}{r_{\rm vir}}; \qquad \text{(A17)}$$

this equals the circular velocity averaged over the halo, which in turn equals $2K_{\rm Iso} = -W_{\rm Iso}$.

A3 The truncated NFW profile

We could go through a similar exercise for a truncated Hernquist profile. Instead, we will study another profile which declines slightly less steeply at the edge, and so is able to fit the results of numerical simulations slightly better (Navarro, Frenk & White 1997). The NFW profile contains mass m within $r_{\rm vir}$, and it is truncated at this scale. Within the virial radius,

$$\frac{\rho(r)}{\bar\rho} = \frac{\Delta_{\rm vir}}{3\Omega}\frac{f(a)}{a^3 x\,(1+x)^2} \qquad \text{(A18)}$$

where $x = r/a$, with $s = r/r_{\rm vir}$ as before, a is the core radius in units of $r_{\rm vir}$, and

$$f(a) = \Big[\ln(1+1/a) - 1/(1+a)\Big]^{-1}. \qquad \text{(A19)}$$

The potential at r is

$$\phi(r) = -\frac{Gm}{r_{\rm vir}}\,\frac{f(a)}{a}\,\left[\frac{\ln(1+x)}{x} - \frac{a}{1+a}\right]. \qquad \text{(A20)}$$

The corresponding expression in Cole & Lacey (1996) does not have the second term in the square brackets because we are assuming the halo is truncated at the virial radius, whereas they did not. The circular velocity is

$$v_{\rm c}^2(r) = \frac{Gm}{r_{\rm vir}}\,\frac{f(a)}{a}\,\left[\frac{\ln(1+x)}{x} - \frac{1}{1+x}\right], \qquad \text{(A21)}$$

and the total potential energy is

$$W_{\rm NFW} = -\frac{Gm^2}{2\,r_{\rm vir}}\,\frac{f(a)^2}{a(1+a)}\left[1 - 2a\ln(1+1/a) + \frac{a}{1+a}\right]. \qquad \text{(A22)}$$

for the truncated potential given above. This equals the average of the circular velocity over the halo. If the halo is not truncated (equation A20 without the second term in the square brackets), then the total potential energy is $W_{\rm NFW} = -(Gm^2/r_{\rm vir})\,f^2(a)/2$ if we integrate over all r, and it is

$$W_{\rm NFW} = -\frac{Gm^2}{2\,r_{\rm vir}}\,\frac{f(a)^2}{a(1+a)}\,[1 - a\ln(1+1/a)], \qquad \text{(A23)}$$

if we integrate out to $r_{\rm vir}$ only.

The radial velocity dispersion, computed from the Jeans equation, is

$$\frac{\sigma_r^2(r)}{Gm/r_{\rm vir}} = \frac{f(a)^2}{2a}\,\frac{x(1+x)^2}{f(a)}\,\Big[g(1/a) - g(x)\Big], \qquad \text{(A24)}$$

where

$$g(x) \equiv -1 + \frac{1}{x} + \frac{1}{(1+x)^2} + \frac{6}{1+x} + \ln\frac{x}{1+x} + \frac{6x^2+3x-1}{x^2(1+x)}\ln(1+x) - 3\ln^2(1+x) + 6{\rm Li}_2(x):$$

the dilogarithm ${\rm Li}_2(x)$ is defined by

$${\rm Li}_2(x) \equiv \int_0^x {\rm d}\ln z\;\ln(1+z).$$

This, in the expression for the total kinetic energy shows explicitly that $-W_{\rm NFW} = 2K_{\rm NFW}$. This relation is satisfied exactly because we truncated the halo at the virial radius. If we do not truncate, and we let the halo extend to infinity, then the expression above should be modified by setting $g(1/a) \to \pi^2 - 1$.

The convolution of such a profile with itself gives

$$\begin{aligned}\frac{4\pi r_{\rm vir}^3 a^3}{m^2}\,\frac{\lambda_{\rm NFW}(r|m,a)}{f(a)^2} &= \frac{-4(1+a)+2ax(1+2a)+a^2x^2}{2x^2(1+a)^2(2+x)} \\ &\quad + \frac{1}{x^3}\ln\left[\frac{(1+a-ax)(1+x)}{(1+a)}\right] \\ &\quad + \frac{\ln(1+x)}{x(2+x)^2} \quad \text{if } 0\le s\le 1 \\ &= \frac{\ln[(1+a)/(ax+a-1)]}{x(2+x)^2} + \frac{a^2x-2a}{2x(1+a)^2(2+x)} \\ &\qquad \text{if } 1\le s\le 2. \qquad \text{(A25)}\end{aligned}$$

In the limit in which the virial radius is much larger than the core radius, this separates into the product of a function of a and another of x:

$$\lambda_{\rm NFW}(r|m,a) \;\to\; \frac{m^2\,f(a)^2}{4\pi r_{\rm vir}^3 a^3}\,\frac{2}{x^2(x+2)} \times \left[\frac{(x^2+2x+2)\ln(1+x)}{x(x+2)} - 1\right].$$

Straightforward but tedious algebra shows that the integral of $2\pi G r^2\,\lambda_{\rm NFW}(r|m,a)/r$ equals $W_{\rm NFW}$, the average of the potential over the halo. Again, this equality is exactly satisfied only because we have self-consistently truncated our haloes (equations A25 and A22).

It is an interesting question as to whether or not truncation is important. Although they discuss NFW haloes truncated at the virial radius (so they have finite mass) it appears that Cole & Lacey (1996) do not truncate their NFW haloes when computing ϕ and σ_r. As a result, their values of σ_r do not go to zero at the virial radius, and their values

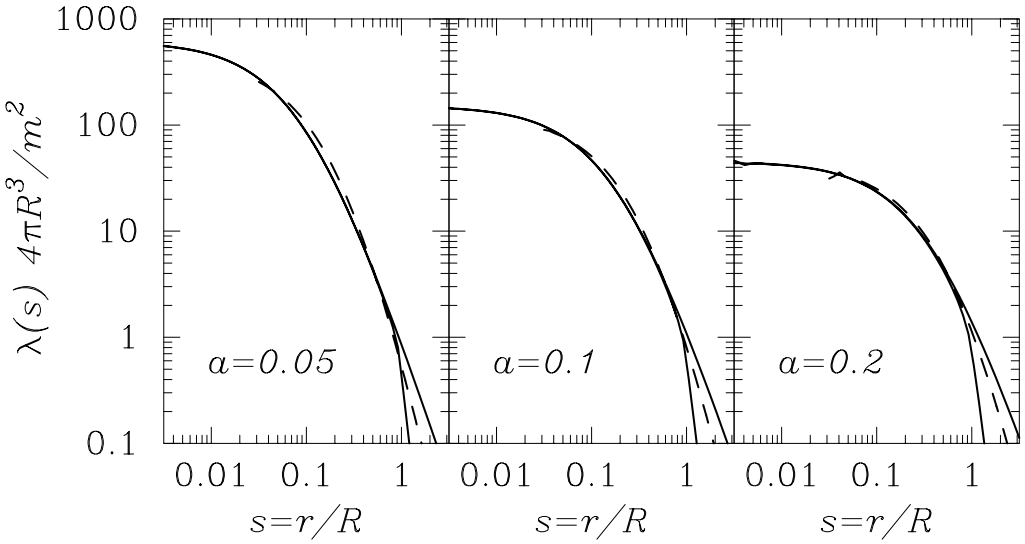

Figure A1. Shape of the convolution of the density profile as a function of distance in units of the virial radius for a few representative values of the core radius a. Small values of a (left panel) correspond to low mass haloes, whereas more massive haloes have larger core radii (right panel). Solid curves show the result for NFW haloes truncated at the virial radius (lower amplitude at large r) and when the haloes are allowed to extend to infinity (larger amplitude at large r), and dashed curves show the corresponding result for a Hernquist profile which contains the same mass within the virial radius. The core radius of the Hernquist profile is $\sqrt{2}\,a^{0.75}$.

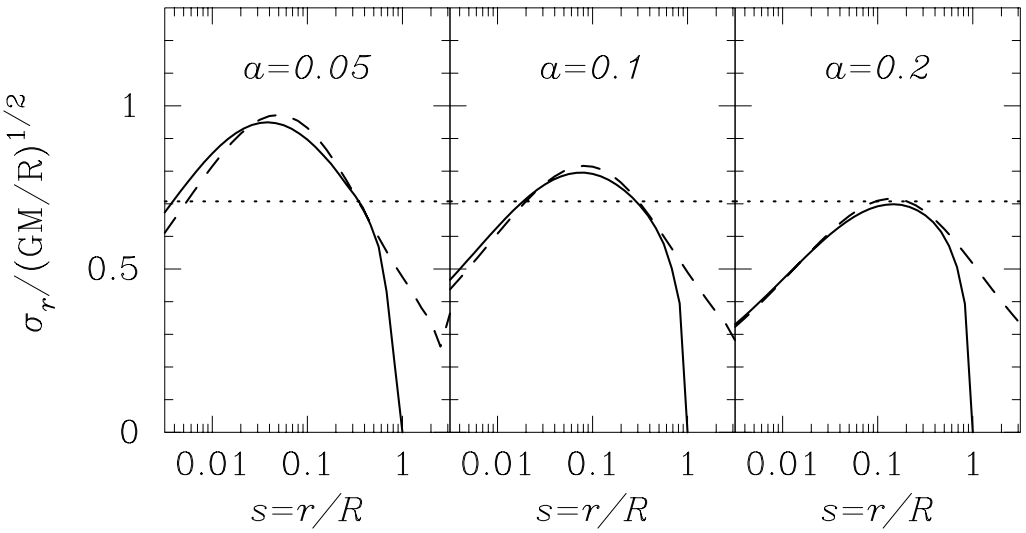

Figure A2. Radial velocity dispersion as a function of distance from halo centre if orbits are isotropic for the same models as the previous figure. Solid curves show the dispersion in NFW haloes truncated at the virial radius, dotted curves show the isothermal value (which is independent of distance from centre) and dashed curves show the result for the corresponding Hernquist profile.

of $W_{\rm NFW}/2K_{\rm NFW}$ at the virial radius are slightly greater than unity. Both these are in agreement with the simulation results they present. Since NFW haloes are not really isolated objects, it may be that Cole & Lacey's decision to ignore the truncation at the virial radius when computing all quantities except the mass is more physically reasonable.

Deciding whether to truncate or not is important if one wishes to include the scale dependence of the velocity dispersion within a halo into our model for the pairwise velocity dispersion. We found that using our formula for truncated NFW haloes, and then integrating over the distribution of halo masses produced values of σ_{12} which were about 15% lower than the simulation results presented in Fig. 5. If we do not truncate, our models are better able to reproduce the measurements in simulations, suggesting that this is, indeed, the correct thing to do.

The solid curves in Fig. A2 show the radial velocity dispersion as a function of radius for truncated NFW haloes (eq. A24) for three representative values of the concentration parameter a; panels on the left correspond to the least massive haloes. The dotted curves show the isothermal value: one half of $GM/r_{\rm vir}$, and dashed curves show the corresponding result for an infinite Hernquist profile, with core radius $b = \sqrt{2}\,a^{0.75}$. With this scaling, the Hernquist formula for the dispersion provides a good approximation to what happens if we remove the condition that the NFW

profile is truncated. This is useful because the Hernquist radial velocity profile is analytic.